Substantial cold bias during wintertime cold extremes in the southern Cascadia region in historical CMIP6 simulations

Rogers, M.H.[1], **Mauger, G.**[1], **Cristea, N.**[2]

[1]Climate Impacts Group, University of Washington
[2]Department of Civil & Environmental Engineering, University of Washington

Key Points:

- CMIP6 models show a pronounced cold bias in the coldest daily minimum temperatures for the Cascadia region of North America.
- In both the ERA5 and CMIP6 models, the coldest temperatures in this region are associated with atmospheric blocking patterns in the northeast Pacific.
- Due to their poorly resolved topography, CMIP6 models allow excessive advection of cold continental air during atmospheric blocking events

Corresponding author: Matthew Rogers, `rawrgers@uw.edu`

Abstract

Global climate models often simulate atmospheric conditions incorrectly due to their coarse grid resolution, flaws in their dynamics, and biases resulting from parameterization schemes. Here we document the magnitude and extent of minimum temperature biases in the CMIP6 model ensemble, relative to ERA5. Bias in the southern Cascadia region (i.e. Pacific Northwestern United States and southwestern British Columbia, Canada, spanning from the coast to the Rocky Mountains) stands out relative to the rest of North America, with some models showing a bias in excess of -10°C in the 1st percentile of daily winter minimum temperature. During the coldest minimum temperature days, the CMIP6 models show an anomalous high in mean sea level pressure in the Northeast Pacific – an atmospheric blocking pattern that is also present in ERA5. While this atmospheric blocking pattern is typically concurrent with cold temperatures across much of North America, terrain barriers such as the Rockies and Cascades prevent the cold air from reaching the Pacific Northwest in observation and reanalysis. Our results suggest that the bias in CMIP6 minimum temperatures is a result of unresolved topography in the Rockies and Cascade mountain ranges, such that the terrain does not adequately block cold air advection from the interior of the continent.

Plain Language Summary

Global climate models, for a variety of reasons, continue to struggle with recreating some of the observed behaviors of our Earth system. Here, we document one such issue: daily minimum temperatures in western Washington and Southwestern British Columbia that are much colder than we experience. We find that these temperatures occur when extremely cold air is moved from the north into western Washington and southwestern British Columbia. In reality, terrain barriers such as the Rocky and Cascade mountain ranges prevent this air from reaching western Washington and southwestern British Columbia. However, these mountain ranges in the models are much lower and less jagged, which allows the extreme cold temperatures to occur in the models.

1 Introduction

Global climate model (GCM) projections of future climate conditions are extensively used in analyses of climate change impacts. GCMs are the primary source of future climate projections, and are the basis for the majority of impact assessments used to inform decision-makers about potential future climate conditions(e.g. Reidmiller et al., 2018). Projected climate change is expected to significantly impact society by affecting necessary aspects such as water availability, human health , and food security Reidmiller et al. (2018). Thus, providing decision-makers with reliable estimates of present and future conditions is crucial for them to make well-informed decisions about future climate-related risks.

Many studies have evaluated GCM performance by using historical simulations as a benchmark to compare to observations and reanalysis data (e.g. Rupp et al., 2013). As a result of such evaluations, GCMs have significantly improved in their simulations of observed atmospheric phenomena in recent years (Edwards, 2011; Sillmann et al., 2013; Flato et al., 2013a). GCMs have shown fidelity in simulating global quantities , and yet continue to have considerable bias on regional scales Flato et al. (2013b) due to a variety of factors, including coarse grid resolution, flaws in their dynamics, and biases resulting from parameterization schemes (Taylor et al., 2012; Knutti & Sedláček, 2013; O'Gorman & Schneider, 2009; Wilcox & Donner, 2007; Wehrli et al., 2018). GCM bias at regional scales presents a barrier for decisions-makers in being well-informed on current and future climate conditions. Further assessment of regional GCM bias is important for understanding how reliable GCM simulations are and to what extent they can be utilized.

In a preliminary investigation of Coupled Model Intercomparison Project Phase 5 (CMIP6) models, we found that simulated cold extremes in Puget Sound were often below the range of observed temperature extremes. Further analysis of cold extreme events in these GCMs showed that the cold biases often affected much of the southern Cascadia region (i.e., Pacific Northwestern United States west of the Rockies along with southwestern British Columbia, Canada (Fig. 1). The unrealistic nature of minimum temperature values in these simulations presents a problem for their use in accurately projecting future changes in temperature variability for the Pacific Northwest. Understanding when and why these biases occur is imperative for understanding the appropriate uses and limitations of minimum temperature data provided by these GCMs.

The observed dynamics behind wintertime cold air outbreaks are well-established, with many previous studies connecting significant cold-air outbreaks in the United States with atmospheric blocking patterns in the Northeast Pacific (e.g. Carrera et al., 2004). Atmospheric blocking regimes in the Northeast Pacific, characterized by a persistent anticyclonic flow anomaly over the gulf of Alaska (Dole, 1986b,a; Higgins & Schubert, 1996; Higgins & Mo, 1997), inhibit the eastward progression of synoptic disturbances through strong meridional flow. This leads to anomalies in the North Pacific storm tracks (Nakamura & Wallace, 1990) that ultimately advect cold air southward into the United States. Carrera et al. (2004) show that average daily temperature anomalies are consistently below the 10^{th} percentile over an area stretching from British Columbia southeastward to the central plains of the United States when a North Pacific blocking event occurs. More recently, the connections between severe cold conditions during the winter of 2013-14 have also been correlated with an atmospheric blocking pattern in the Northeast Pacific Hartmann (2015).

For North America specifically, winter stationary wave patterns resulting from orography also have a significant impact on wintertime temperature variability; resulting from their influence on horizontal temperature advection Held et al. (2002). Horizontal temperature advection is known to be the largest contributor to synoptic temperature variability in the Northern Hemisphere Lutsko et al. (2019), and previous research suggests that terrain plays an important role in how cold air is advected into the United States Hartjenstein & Bleck (1991), particularly during atmospheric blocking events in the Northeast Pacific.

Taken together, the known interactions between the atmospheric dynamics and terrain that lead to cold temperatures in southern Cascadia present two possibilities for the existence of the cold temperature bias in the southern Cascadia region. Namely, biases in the strength and location of North Pacific atmospheric blocking events leading to stronger cold advection into Pacific Northwwest North America, and bias in terrain simulation in the CMIP6 models that allows cold air to reach areas it normally would not in observation. With this, our study has two objectives; (1) to document the magnitude and spatial extent of bias in cold minimum temperatures in the southern Cascadia region of North America and, (2) to identify when this bias occurs and assess the relative contributions to this bias from the atmospheric dynamic and terrain bias. Given the localized nature of the bias to the southern Cascadia region, we hypothesize that the biases in extreme daily minimum temperatures in CMIP6 models are related to bias in terrain features allowing cold air to move west of the Rocky and Cascade mountain ranges during North Pacific atmospheric blocking events.

2 Data & Methods

We use daily mean sea level pressure, daily minimum temperature data, and grid cell elevation data from historical simulations of 13 CMIP6 global climate models (Table 1), obtained using the Pangeo cloud storage platform (https://pangeo.io). For validation, we compare the CMIP6 results to data from the European Centre for Medium-

Model	Citation	Native Resolution
ACCESS-CM2	Dix et al. (2019)	1.25° x 1.875°
ACCESS-ESM1-5	Ziehn et al. (2019)	1.875° x 1.25°
AWI-ESM-1-1-LR	Danek et al. (2020)	1.875° x 1.875°
CanESM5	Swart et al. (2019)	2.8125° x 2.8125°
CMCC-ESM2	Lovato et al. (2021)	0.9375° x 1.25°
MIROC6	Tatebe & Watanabe (2018)	1.40625°x 1.40625°
MPI-ESM1-2-LR	Wieners et al. (2019)	1.875° x 1.875°
MPI-ESM1-2-HR	Jungclaus et al. (2019)	0.9375° x 0.9375°
MRI-ESM2-0	Yukimoto et al. (2019)	2.8125° x 2.8125°
NorCPM1	Bethke et al. (2019)	1.875° x 2.5°
NorESM2-MM	Bentsen et al. (2019)	0.9375° x 1.25°
SAM0-UNICON	Park & Shin (2019)	0.9375° x 1.25°
TaiESM1	Lee & Liang (2019)	0.9375° x 1.25°

Range Weather Forecasts Reanalysis version 5 (ERA5) Hersbach et al. (2020), which was chosen for its fine default resolution of 0.25° x 0.25° latitude by longitude grid and overall reliability as an accurate reanalysis produce Tarek et al. (2020). All data was regridded to a 1°x1° latitude by longitude grid via bilinear interpolation unless otherwise noted, and all reported bias for the CMIP6 models is relative to ERA5 data.

We evaluate biases in the 1st percentile of daily minimum temperature in order to ensure an adequate sample size for the selected time period (1981-2010), though our analysis indicates that the results would be the same for a variety of definitions of cold minimum temperatures. Hereafter we refer to values below the 1st percentile threshold as "extreme cold".

3 Results

Our results are divided into two sections. The first section focuses on the documentation of extreme minimum temperature bias, its spatial extent and how pervasive it is across CMIP6 models. The second section investigates the source of wintertime extreme minimum temperature bias in the southern Cascadia region in CMIP6 models.

3.1 Bias Documentation

Preliminary findings have shown isolated events with minimum temperatures well below observed values in the Puget Sound region; however, the extent and magnitude of this bias has yet to be assessed. Fig. 1a shows the bias in the multi-model mean 1st percentile minimum DJF temperature (1981-2010) for CMIP6 models relative to ERA5 for North America. The bias in the southern Cascadia region extending southeast into the mountain west region stands out relative to the rest of North America, excluding perhaps the southern coast of Alaska. The magnitude of the extreme minimum temperature bias for several grid cells within this region shows an ensemble average bias exceeding -5°C, which is a stark departure from observed values. Fig. 1b shows that the sign of the bias is the same for all CMIP6 models analyzed, without exception. These results suggest two things: (1) CMIP6 models have a systematic problem in simulating realistic extreme cold air in the southern Cascadia region; and (2) the source of this bias is likely specific to this region, given that biases in other regions are not as large, are not necessarily of the same sign, and show less consistency among models. Hereafter, our analysis will be focused on this region, though we note that there are other regions with similar bias characteristics (e.g., southeastern Alaska). We select a sub-region that isolates

the largest magnitude and agreement in the sign of bias in the CMIP6 ensemble (Fig. 1a, b: 46.5N - 51.5N, 125W - 116W).

Our first goal is to determine whether the bias in the minimum temperature is unique to the coldest temperatures or is present throughout the entire distribution of wintertime minimum temperatures. Fig. 2a compares the probability distributions of daily wintertime minimum temperatures (1981-2010) averaged over the southern Cascadia region for ERA5 and the CMIP6 models. The daily minimum temperature distributions for most models shown in Fig. 2a are more left skewed relative to ERA5, meaning that CMIP6 models in this region consistently simulate colder minimum temperatures than in the observations. This does not appear to be a result of a shifted distribution, since the right tail of the distributions are similar. Instead, the bias appears to be confined to the lower end of the minimum temperature distributions in ERA5 and CMIP6 models. The cold bias is consistently present across a range of the lower quantiles in the distribution, but begins to be less consistently negative around the XXth percentile.

To better visualize how the bias in 1st percentile minimum temperatures compares to bias in the median, Fig. 2b shows the bias in 50th percentile and 1st percentile daily minimum wintertime temperatures for each model in this study, averaged over the suthern Cascadia region. Consistently across the ensemble, the bias in the 1st percentile minimum temperatures far exceeds the bias in the median for the southern Cascadia region, again suggesting that the distributions for minimum temperature in CMIP6 models for the southern Cascadia region are skewed left relative to ERA5. Notably, the absolute magnitude of the 1st percentile bias for many models exceeds -10°C. The results show highly skewed probability distributions (Fig. 2a) and a larger magnitude of bias in the 1st percentiles relative to the median relative to ERA5, suggesting that the bias in extreme minimum temperatures is uncoupled from systematic bias in the minimum temperature distributions.

We have shown that a large bias in minimum temperature extremes for the CMIP6 models is isolated to the southern Cascadia region (Fig. 1). We have also demonstrated that this bias in minimum temperatures is unique to the cold extremes (Fig. 2). Next, we investigate potential sources for this minimum temperature bias

3.2 Sources of Cold Minimum Temperature Bias

Informed by previous research focused on cold temperatures in North America, we hone in on two potential contributors to the cold minimum temperature bias in southern Cascadia in the CMIP6 models: (1) biases in the strength and location of North Pacific atmospheric blocking events, and (2) bias in terrain simulation in the CMIP6 models. We begin this section by analyzing (1).

To investigate the role of cold air advection in the southern Cascadia extreme minimum temperature bias we start by identifying the associated synoptic weather patterns in the models and reanalysis. Fig. 3 shows a composite of mean sea level pressure (MSLP) anomalies relative to DJF average (1981-2010) during days with minimum temperature below the 1st percentile. Results for both ERA5 and the CMIP6 multi-model mean show large areas of positive MSLP anomalies over Alaska and the Gulf of Alaska, which is consistent with the Northeast Pacific atmospheric blocking pattern we would expect during the coldest temperatures over much of North America. The CMIP6 multi-model mean shows anomaly magnitudes less than ERA5, but, upon further investigation, this is a result of the CMIP6 models simulating slightly different positions of the block and not a result of a deficiency in simulated anomaly magnitude. The similarities between the anomaly patterns in Fig. 3 indicates that the CMIP6 models capture the synoptic MSLP anomaly pattern associated with the coldest minimum temperatures in the southern Cascadia region. The similar patterns suggest that the associated synoptic-scale conditions are simulated accurately by the CMIP6 models. Thus, we infer that the primary cause of the

bias is not the synoptic-scale weather patterns but how they manifest conditions at the surface.

To further investigate whether synoptic patterns during the coldest days in the southern Cascadia region in ERA5 and the CMIP6 models are similar, we compare MSLP anomalies over Alaska against minimum daily temperatures in the southern Cascadia region (Fig. 4). MSLP anomalies are averaged over an area encompassing the largest anomalies, as outlined in Fig. 3. The range of pressure anomalies in CMIP6 models is much more consistent with the range in ERA5, though the largest anomalies are slightly higher than in ERA5 and the mode of the distribution is lower. In contrast, the minimum temperature anomalies have very different distributions. In particular, the lowest temperatures in the CMIP6 models are up to 10°C colder than in ERA5, primarily occurring when the maximum SLP anomalies over Alaska are large. Taken together, the similarities in SLP magnitudes (Fig. 4) and patterns (Fig. 3) in the CMIP6 models and ERA5, along with the differences in minimum temperature anomalies, suggest that incorrect simulation of dynamics is not the primary cause of the minimum temperature bias. If incorrect simulation of underlying dynamics of cold minimum temperatures were the cause of this bias, we would expect to see considerable differences in the SLP anomaly pattern or magnitude, or both.

Since the minimum temperature biases are large (some exceeding -10°C, Fig. 2) despite no major biases in dynamics, we have hypothesized that how temperature advection manifests at the surface plays the main role in driving the bias. A previous evaluation of land surface energy fluxes in the CMIP6 models do not identify the southern Cascadia region as having significant bias in sensible, latent, or ground heat flux Li et al. (2021), again suggesting that cold air advection is the primary explanation for the extreme minimum temperature bias. To examine this more closely, we estimate the hourly contributions of the diabatic and adiabatic terms of the temperature tendency formula Holton & Hakim (2013) to identify relative contributions to temperature change leading up to the 10 coldest minimum temperature days (SI 1). Of the select GCMs, all five models (BCC-CSM2-MR, BCC-ESM1, CanESM5, CMCC-ESM1, NorCPM1) analyzed indicate that the primary driver of cold temperatures is cold air advection. Further, some of the GCMs indicate minimum values of temperature advection upwards of -2°C/hr, which is considerably more than shown in ERA5. Taken together, the synoptic MSLP patterns (Fig. 3), the distribution of pressure anomalies versus minimum temperatures (Fig. 4), and the contribution of temperature advection to temperature change in the southern Cascadia region (SI 1), all of the evidence suggests that anomalous cold air advection is the primary cause of the extreme minimum temperature bias in CMIP6 models. Thus, we shift our focus to potential contributor (2), bias in terrain simulation in the CMIP6 models.

Topographic barriers play a large role in the spatial distribution of cold temperatures during cold air outbreaks. This means that some bias in extreme minimum temperatures is likely associated with the coarse resolution of CMIP6 models and the resulting inadequacy in resolving the elevation profile of the southern Cascadia region. Fig. 5 shows the terrain elevation for western North America for ERA5 and CMIP6. Similar to the results from (Mahony et al., 2021), the terrain in the CMIP6 models is much smoother and generally lower in elevation than the terrain in ERA5 (Fig. 5b), especially in Western Washington and the Rockies just northeast of Vancouver Island. The Cascade Range, for example, is essentially missing in the models, while the Rockies are more broad, with a crest that is several hundred meters below the maximum in ERA5.

An elevation cross section through the southern Cascadia region extending into central Canada (Fig. 6; black shading) illustrates the stark difference in the elevation profiles for the CMIP6 models (multi-model mean) and ERA5. The Cascade and Olympic mountain ranges are absent from the CMIP6 elevation profile, and, as shown in Fig. 5, the apex of the Rocky mountains is considerably lower than in ERA5. When overlaid

with the average potential temperature during the coldest percentile in minimum temperature days (Fig. 6; black lines) we see that the west-east potential temperature gradient is relatively small, whereas in ERA5 the gradient between the west and east side of the Cascades and Rocky mountains is large. Furthermore, if we neglect diabatic effects then potential temperature is conserved and can be considered a tracer for air masses as they are advected. Taking this angle, we focus on the 260K potential temperature contour in Fig. 6. In ERA5, this contour is confined to the east of the Rockies and Cascades, while in the CMIP6 models this contour extends all the way to the coast. This suggests that the cold air mass with potential temperature of 260K, when advected into the region, was able to advect over the terrain to the coast of the southern Cascadia region in the CMIP6 models, whereas in ERA5 the cold air was unable to be advected to the coast.

4 Discussion & Conclusions

This study identified bias in extreme minimum temperatures in the southern Cascadia region of North America in the CMIP6 models, which we showed were a likely result of unresolved terrain features. Our results suggest the bias is unique to the region given the high level of agreement and magnitude of the bias in 1st percentile wintertime daily minimum temperatures (Fig. 1). We also showed that the median bias is not consistent with the bias in extreme minimum temperatures for all models, indicating that the bias is due to a misrepresentation of the mechanisms affecting the coldest events in this region.

Prior research on synoptic weather patterns has shown that cold temperatures across North America are associated with atmospheric blocking patterns in the Northeast Pacific. We confirm that both the ERA5 and CMIP6 models show synoptic MSLP patterns that are consistent with this finding (Fig. 3). Additional analysis shows that the MSLP distributions for CMIP6 are similar to those for ERA5 over Alaska and the northeast Pacific (Fig. 4). While the magnitudes of the MSLP anomalies in Alaska are similar in ERA5 and the CMIP6 models, the coldest minimum temperatures in the southern Cascadia region are considerably colder in CMIP6 models relative to ERA5. The highly localized nature of the bias, the demonstrated association with atmospheric blocking in the Northeast Pacific (Figs. 3, 4), and the relative absence of diabatic influences on temperatures during these events all point to errors in simulating cold air advection across the Cascade and Rocky mountain ranges. This is consistent with previous studies showing the importance of terrain in influencing how cold air is advected into North America during atmospheric blocking events in the Northeast Pacific.

The CMIP6 multi-model mean orography showed that models under-resolve the Cascade and Rocky mountains. A horizontal cross section across this domain confirmed that GCM topography differs substantially from actual elevations. Potential temperature contours composited over the coldest minimum temperature days showed the coldest air being confined to the east of the Rockies in ERA5. The same cross section in CMIP6 shows that this cold air mass is much less restricted due to inadequate representation of the terrain barriers, resulting in a significantly diminished temperature contrast between the maritime vs continental sides of each range. Taken together, the results again suggest that adequate resolution of the terrain is needed to accurately simulate extreme minimum temperatures in the southern Cascadia region of North America.

There are several limitations to this study. The number of models used in this study was limited to 13, with only 3 having the hourly temperature and wind data needed to estimate temperature advection during extreme minimum temperature events. In order to make a generalized statement about all CMIP6 models, and confidently rule out potential contributions from diabatic heating, more CMIP6 results would need to be analyzed.

Further, this study did not consider the role of ocean-atmosphere interactions on cold minimum temperatures, which are likely to exhibit a controlling factor on temperature variations in the southern Cascadia region. While latent and sensible heat fluxes contribute to the diabatic term of the temperature tendency formula (SI XXX), the lack of hourly data for the CMIP6 models limits our analysis of how this contributes to extreme minimum temperatures in the southern Cascadia region. It is likely, however, that given the coarse resolution of the CMIP6 models, heat fluxes from complex bays such as Puget Sound are under-represented. Indeed, Fig. 6 appears to show warmer potential temperatures west of the Cascade mountain range in ERA5 compared to the CMIP6 models, which may be evidence of Puget Sound's moderating influence. Although the evidence suggests that cold air advection is a primary driver of extreme wintertime minimum temperature bias in the CMIP6 models, a secondary explanation could be related to CMIP6 model representation of marine air influence in the southern Cascadia region. This may be one reason the cold biases are greater west of the Cascades than they are between the Cascades and the Rockies. Future work could use GCM surface fluxes to estimate the relative contributions of diabatic heating relative to cold advection.

Resources for assessing future climate change are largely limited to the climate change simulations produced for the Coupled Model Intercomparison Projects. In order to plan for climate change impacts it is particularly important to identify and address GCM biases. Strategies to address the extreme minimum temperature bias could include finer resolution GCM simulations, dynamical downscaling over a domain that encompasses all relevant topography, and analyses of historical events to understand the relationships between large-scale conditions and extreme minimum temperatures in the southern Cascadia region. To better elucidate the causes of this bias, future GCM simulations should include the hourly fields needed to estimate the temperature tendency: At a minimum, hourly wind and temperature data, and ideally also latent, sensible, and radiative fluxes at the surface. Finer spatial scales may eliminate the issue of the cold minimum temperature bias altogether if it captures terrain features in Cascadia sufficiently.

Alternatively, statistically or dynamically downscaling could be designed to better capture extreme minimum temperatures. In order to address the issue, downscaling approaches would need to be designed so as not to erroneously pass along biases from the input GCM data . For the minimum temperature bias documented here, the bias for southern Cascadia was originally discovered in dynamically downscaled CMIP5 data. In the case of these simulations, the domain of the downscaling covered the US Pacific Northwest, but did not extend far enough north to capture the topography of the Canadian Cascades and Rockies, and therefore could not correct for the anomalous cold advection through this topography in the GCMs.

In the meantime, communities needing to plan for changes in extreme cold conditions are limited by a lack of suitable GCM or downscaled projections. In areas where the extreme minimum temperature bias is present, stakeholders should consider alternative approaches to assessing impacts. Alternatives could include sensitivity testing in order to identify thresholds for impact, assuming that extreme minimum temperatures warm at the same rate as the annual or seasonal average temperature, or assessing trends from observations. While GCMs remain the primary information resource for preparing for climate change, these alternatives can provide decision-makers with important information to help them prepare for the impacts of climate change.

5 Open Research

CMIP6 data used in this study was accessed using the Pangeo cloud catalog (https://pangeo.io) (Abernathey et al., 2017), and ERA5 data is available for download from the Copernicus climate data store (https://cds.climate.copernicus.eu) (Hersbach et al., 2020). Figures in this study were created with Matplotlib version 3.4.3, available at https://matplotlib.org/.

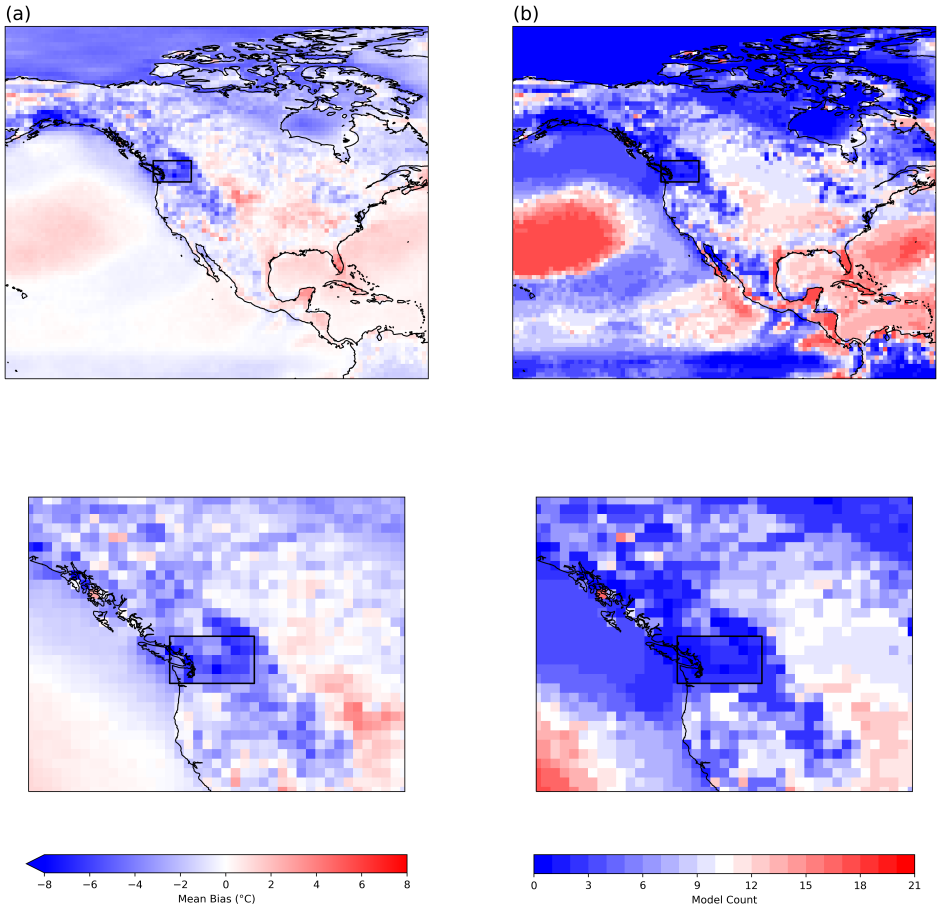

Figure 1. (column a) multi-model mean bias in 1st percentile daily minimum winter (DJF) temperature (1981-2010) for 13 CMIP6 models relative to ERA5, and (column b) model agreement on positive sign of bias. The black boxes denote the area of interest for this study (46.5°N-51.5°N,125°W-116°W)

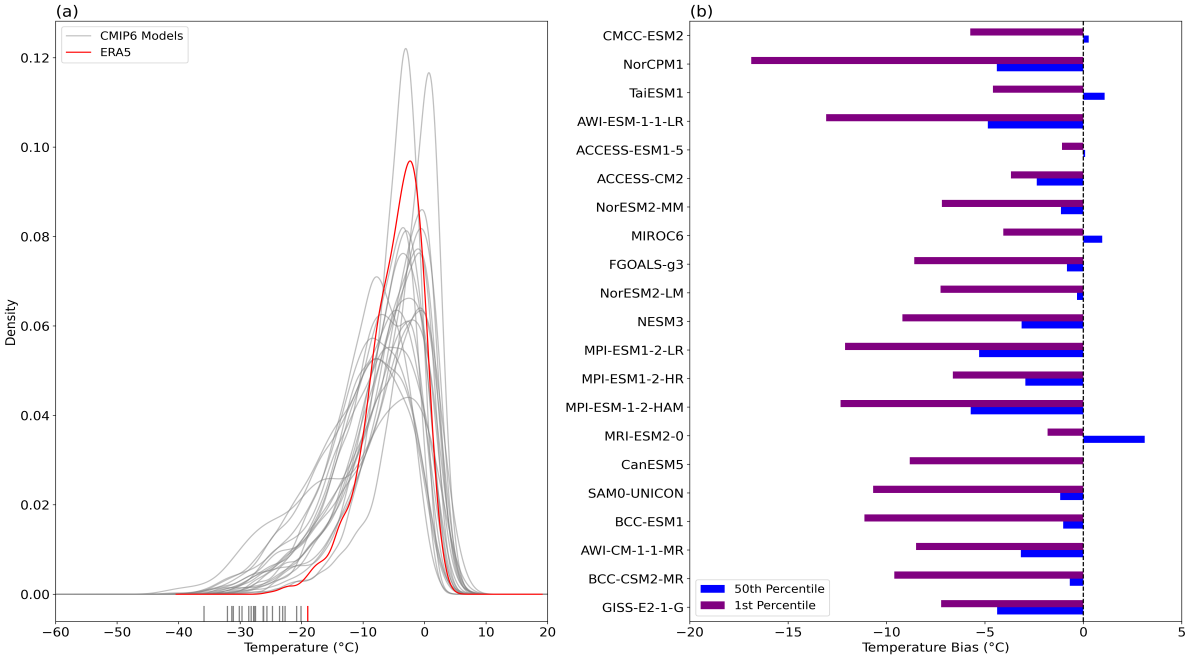

Figure 2. (a) Probability density functions (PDFs) of DJF daily minimum temperatures (°C) averaged over the domain 46.5N - 51.5N and 125W - 116W for 13 CMIP6 models (gray) and ERA5 (red) from 1981-2010, and (b) individual CMIP6 model bias in the 1st (purple) and 50th (blue) percentile daily minimum temperature (°C) over the same domain and time period as (a).

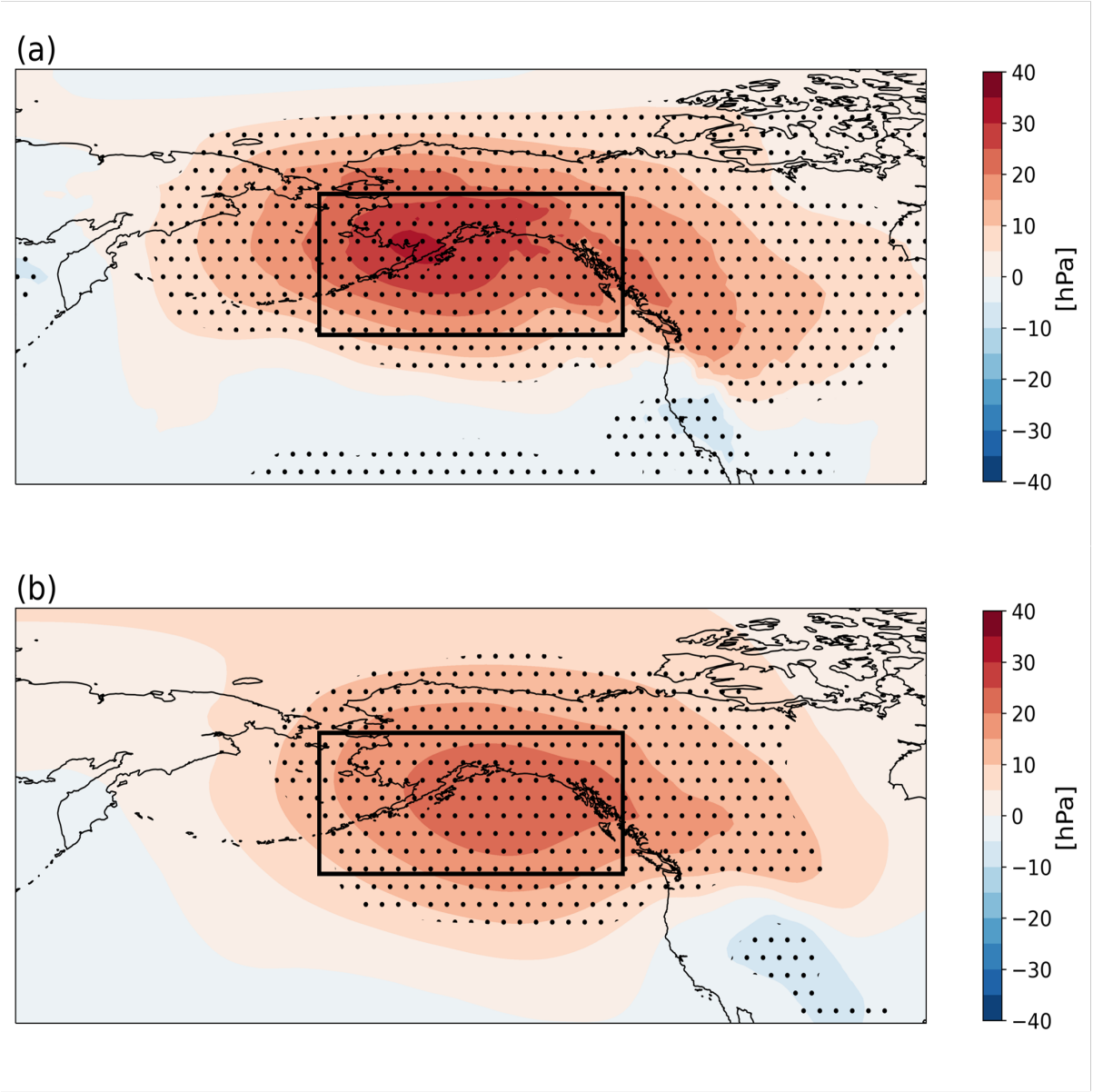

Figure 3. (a) Composite mean sea level pressure anomalies (MSLP; hPa) during days when the average minimum temperature in the PNW region is below the 1st percentile for ERA5, and (b) multi-model mean composite MSLP anomalies during days when the average minimum temperature in the PNW region is below the 1st percentile for the CMIP6 models . Black stippling indicates statistical significance at the 95% confidence level using a bootstrapping method with 1000 iterations. Black box indicates the region of interest for investigating MSLP anomalies is the next analysis.

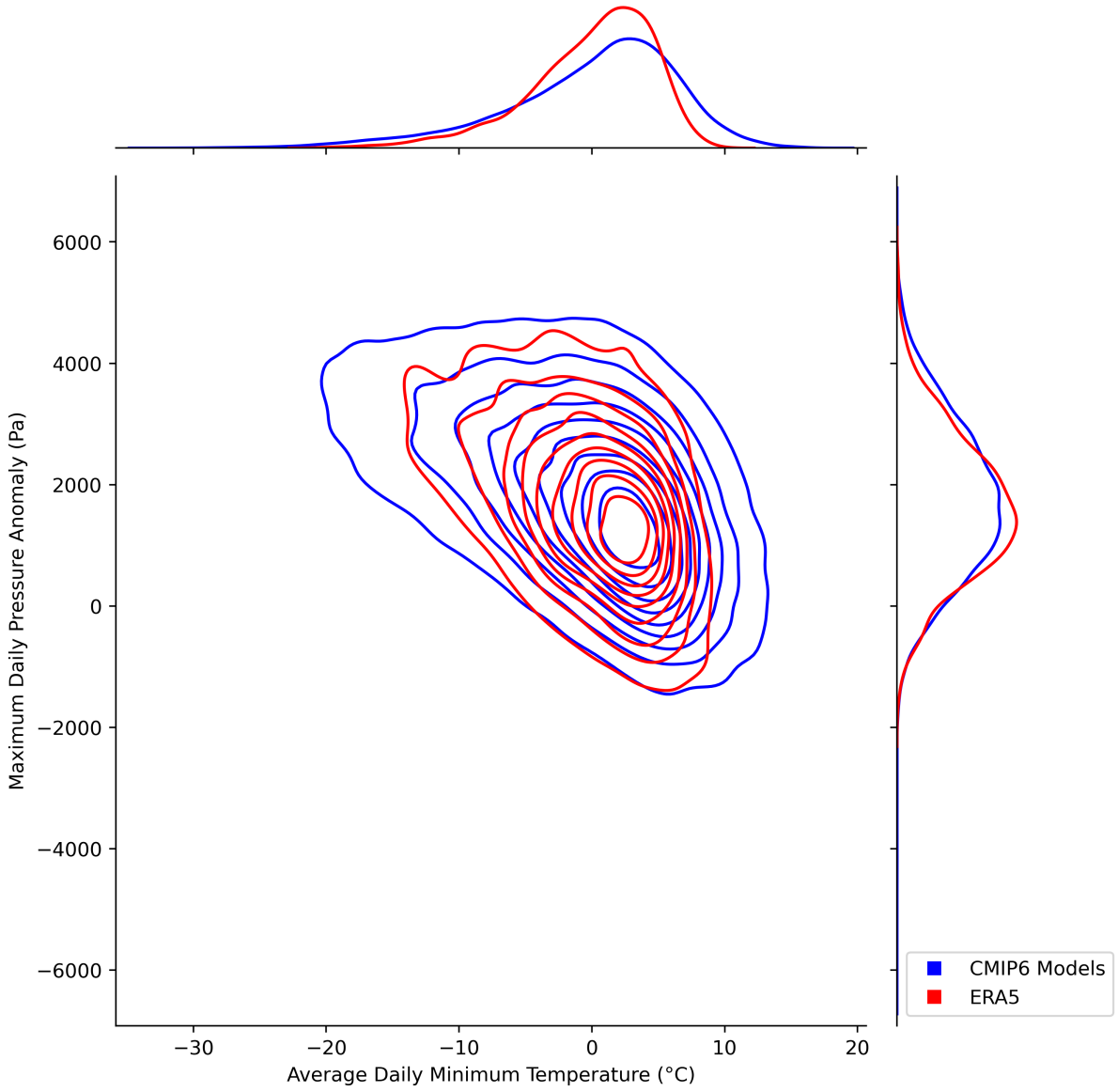

Figure 4. Density plot of daily minimum temperature averaged over the southern Cascadia region ((46.5°N-51.5°N,125°W-116°W)) vs. the minimum daily MSLP anomalies over the Gulf of Alaska (48°N-67°N,190°W-230°W) for the days below the 1st percentile minimum daily temperature in the southern cascadia region. ERA5 data is in red and the 13 CMIP6 models are in blue. External probability functions are shown for daily minimum temperatures (x-axis; top) and minimum dails MSLP anomalies (y-axis; top).

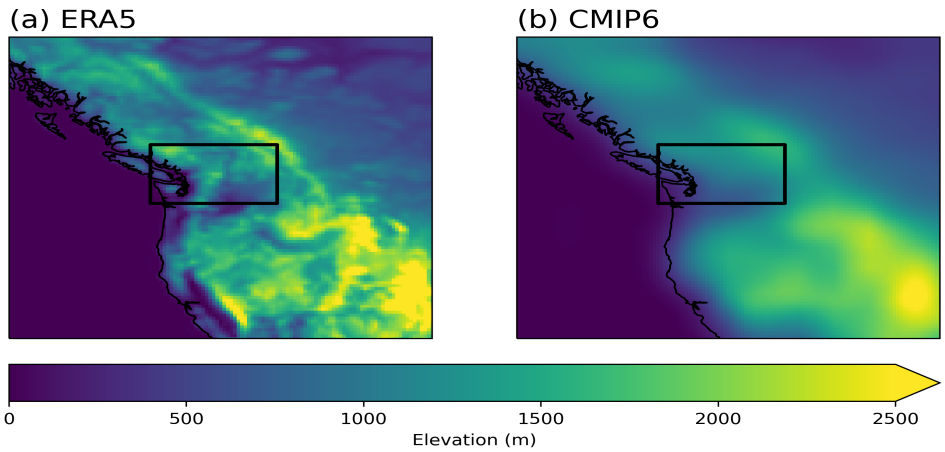

Figure 5. Elevation of grid cells in (a) ERA5 and (b) CMIP6 multi-model mean. CMIP6 grids were interpolated to the ERA5 grid (0.25° latitude x 0.25° longitude) using bilinear interpolation. Area outlined by the black box in each subplot (46.5°N-51.5°N,125°W-116°W) is the southern Cascadia region, or the selected high-bias-high-agreement area.

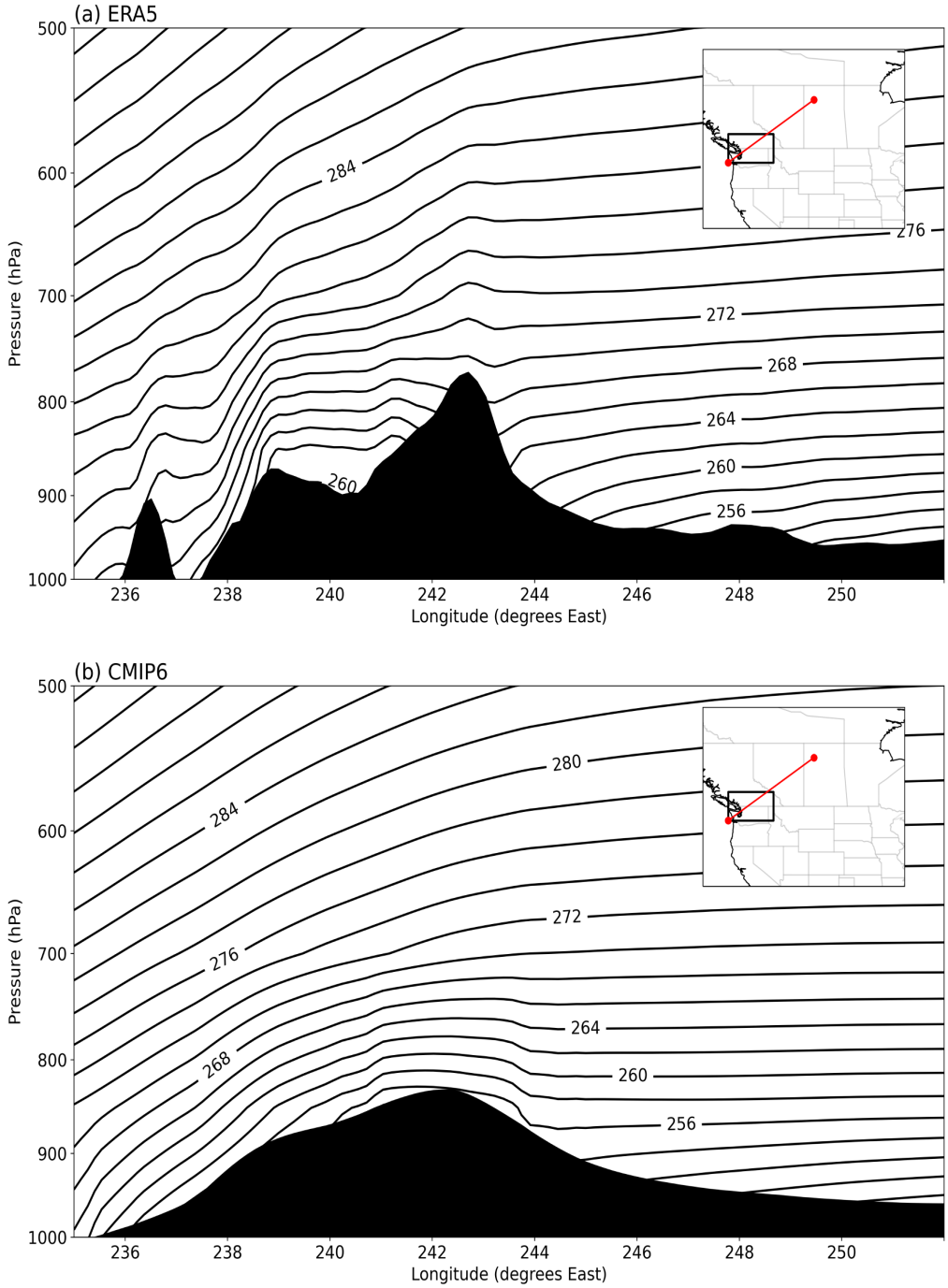

Figure 6. Vertical cross-section (red line) of mean potential temperature (contours) for days below the 1st percentile in spatially-averaged DJF minimum temperature for the area bounded by 46.5°N-51.5°N and 125°W-116°W (black box) for (a) ERA5 and (b) CMIP6 multi-model mean.

References

Abernathey, R., kevin paul, joe hamman, matthew rocklin, chiara lepore, michael tippett, ... Vento, D. D. (2017, 8). *Pangeo nsf earthcube proposal.* Retrieved from https://figshare.com/articles/journal_contribution/Pangeo_NSF_Earthcube_Proposal/5361094 doi: 10.6084/m9.figshare.5361094.v1

Bentsen, M., Oliviè, D. J. L., Seland, y., Toniazzo, T., Gjermundsen, A., Graff, L. S., ... Schulz, M. (2019). *Ncc noresm2-mm model output prepared for cmip6 cmip.* Earth System Grid Federation. Retrieved from https://doi.org/10.22033/ESGF/CMIP6.506 doi: 10.22033/ESGF/CMIP6.506

Bethke, I., Wang, Y., Counillon, F., Kimmritz, M., Fransner, F., Samuelsen, A., ... Keenlyside, N. (2019). *Ncc norcpm1 model output prepared for cmip6 cmip.* Earth System Grid Federation. Retrieved from https://doi.org/10.22033/ESGF/CMIP6.10843 doi: 10.22033/ESGF/CMIP6.10843

Carrera, M. L., Higgins, R. W., & Kousky, V. E. (2004, December). Downstream Weather Impacts Associated with Atmospheric Blocking over the Northeast Pacific. *Journal of Climate*, *17*(24), 4823–4839. Retrieved 2021-08-04, from https://journals.ametsoc.org/view/journals/clim/17/24/jcli-3237.1.xml doi: 10.1175/JCLI-3237.1

Danek, C., Shi, X., Stepanek, C., Yang, H., Barbi, D., Hegewald, J., & Lohmann, G. (2020). *Awi awi-esm1.1lr model output prepared for cmip6 cmip.* Earth System Grid Federation. Retrieved from https://doi.org/10.22033/ESGF/CMIP6.9301 doi: 10.22033/ESGF/CMIP6.9301

Dix, M., Bi, D., Dobrohotoff, P., Fiedler, R., Harman, I., Law, R., ... Yang, R. (2019). *Csiro-arccss access-cm2 model output prepared for cmip6 cmip.* Earth System Grid Federation. Retrieved from https://doi.org/10.22033/ESGF/CMIP6.2281 doi: 10.22033/ESGF/CMIP6.2281

Dole, R. M. (1986a). The life cycles of persistent anomalies and blocking over the north pacific. In B. Saltzman, R. Benzi, & A. C. Wiin-Nielsen (Eds.), *Anomalous atmospheric flows and blocking* (Vol. 29, p. 31-69). Elsevier. Retrieved from https://www.sciencedirect.com/science/article/pii/S0065268708600345 doi: https://doi.org/10.1016/S0065-2687(08)60034-5

Dole, R. M. (1986b). Persistent anomalies of the extratropical northern hemisphere wintertime circulation: Structure. *Monthly Weather Review*, *114*(1), 178 - 207. Retrieved from https://journals.ametsoc.org/view/journals/mwre/114/1/1520-0493_1986_114_0178_paoten_2_0_co_2.xml doi: 10.1175/1520-0493(1986)114⟨0178:PAOTEN⟩2.0.CO;2

Edwards, P. N. (2011). History of climate modeling. *WIREs Climate Change*, *2*(1), 128-139. Retrieved from https://wires.onlinelibrary.wiley.com/doi/abs/10.1002/wcc.95 doi: https://doi.org/10.1002/wcc.95

Flato, G., Marotzke, J., Abiodun, B., Braconnot, P., Chou, S., Collins, W., ... Rummukainen, M. (2013b). Climate change 2013: The physical science basis. contribution of working group i to the fifth assessment report of the intergovernmental panel on climate change. In T. Stocker et al. (Eds.), (chap. Evaluation of Climate Models). Cambridge, United Kingdom and New York, NY, USA: Cambridge University Press.

Flato, G., Marotzke, J., Abiodun, B., Braconnot, P., Chou, S. C., Collins, W., ... Rummukainen, M. (2013a). Climate change 2013: The physical science basis. contribution of working group i to the fifth assessment report of the intergovernmental panel on climate change. In T. F. Stocker et al. (Eds.), (pp. 741–882). Cambridge, UK: Cambridge University Press.

Hartjenstein, G., & Bleck, R. (1991). Factors affecting cold-air outbreaks east of the rocky mountains. *Monthly Weather Review*, *119*(9), 2280 - 2292. Retrieved from https://journals.ametsoc.org/view/journals/mwre/119/9/1520-0493_1991_119_2280_facaoe_2_0_co_2.xml doi: 10.1175/1520-0493(1991)119⟨2280:

FACAOE⟩2.0.CO;2

Hartmann, D. L. (2015). Pacific sea surface temperature and the winter of 2014. *Geophysical Research Letters*, *42*(6), 1894-1902. Retrieved from https://agupubs.onlinelibrary.wiley.com/doi/abs/10.1002/2015GL063083 doi: https://doi.org/10.1002/2015GL063083

Held, I. M., Ting, M., & Wang, H. (2002, August). Northern Winter Stationary Waves: Theory and Modeling. *Journal of Climate*, *15*(16), 2125–2144. Retrieved 2021-10-29, from https://journals.ametsoc.org/view/journals/clim/15/16/1520-0442_2002_015_2125_nwswta_2.0.co_2.xml doi: 10.1175/1520-0442(2002)015⟨2125:NWSWTA⟩2.0.CO;2

Hersbach, H., Bell, B., Berrisford, P., Hirahara, S., Horányi, A., Muñoz-Sabater, J., ... Thépaut, J.-N. (2020). The era5 global reanalysis. *Quarterly Journal of the Royal Meteorological Society*, *146*(730), 1999-2049. Retrieved from https://rmets.onlinelibrary.wiley.com/doi/abs/10.1002/qj.3803 doi: https://doi.org/10.1002/qj.3803

Higgins, R. W., & Mo, K. C. (1997). Persistent north pacific circulation anomalies and the tropical intraseasonal oscillation. *Journal of Climate*, *10*(2), 223 - 244. Retrieved from https://journals.ametsoc.org/view/journals/clim/10/2/1520-0442_1997_010_0223_pnpcaa_2.0.co_2.xml doi: 10.1175/1520-0442(1997)010⟨0223:PNPCAA⟩2.0.CO;2

Higgins, R. W., & Schubert, S. D. (1996). Simulations of persistent north pacific circulation anomalies and interhemispheric teleconnections. *Journal of Atmospheric Sciences*, *53*(1), 188 - 207. Retrieved from https://journals.ametsoc.org/view/journals/atsc/53/1/1520-0469_1996_053_0188_sopnpc_2_0_co_2.xml doi: 10.1175/1520-0469(1996)053⟨0188:SOPNPC⟩2.0.CO;2

Holton, J., & Hakim, G. (2013). *An introduction to dynamic meteorology.* Academic Press, Cambridge. doi: https://doi.org/10.1016/C2009-0-63394-8

Jungclaus, J., Bittner, M., Wieners, K.-H., Wachsmann, F., Schupfner, M., Legutke, S., ... Roeckner, E. (2019). *Mpi-m mpiesm1.2-hr model output prepared for cmip6 cmip.* Earth System Grid Federation. Retrieved from https://doi.org/10.22033/ESGF/CMIP6.741 doi: 10.22033/ESGF/CMIP6.741

Knutti, R., & Sedláček, J. (2013, April). Robustness and uncertainties in the new CMIP5 climate model projections. *Nature Climate Change*, *3*(4), 369–373. Retrieved from https://doi.org/10.1038/nclimate1716 doi: 10.1038/nclimate1716

Lee, W.-L., & Liang, H.-C. (2019). *As-rcec taiesm1.0 model output prepared for cmip6 cmip.* Earth System Grid Federation. Retrieved from https://doi.org/10.22033/ESGF/CMIP6.9684 doi: 10.22033/ESGF/CMIP6.9684

Li, J., Miao, C., Wei, W., Zhang, G., Hua, L., Chen, Y., & Wang, X. (2021). Evaluation of cmip6 global climate models for simulating land surface energy and water fluxes during 1979–2014. *Journal of Advances in Modeling Earth Systems*, *13*(6), e2021MS002515. Retrieved from https://agupubs.onlinelibrary.wiley.com/doi/abs/10.1029/2021MS002515 (e2021MS002515 2021MS002515) doi: https://doi.org/10.1029/2021MS002515

Lovato, T., Peano, D., & Butenschön, M. (2021). *Cmcc cmcc-esm2 model output prepared for cmip6 cmip.* Earth System Grid Federation. Retrieved from https://doi.org/10.22033/ESGF/CMIP6.13164 doi: 10.22033/ESGF/CMIP6.13164

Lutsko, N. J., Baldwin, J. W., & Cronin, T. W. (2019, September). The Impact of Large-Scale Orography on Northern Hemisphere Winter Synoptic Temperature Variability. *Journal of Climate*, *32*(18), 5799–5814. Retrieved 2021-10-29, from https://journals.ametsoc.org/view/journals/clim/32/18/jcli-d-19-0129.1.xml doi: 10.1175/JCLI-D-19-0129.1

Mahony, C., Wang, T., Hamann, A., & Cannon, A. (2021, 06). *A cmip6 ensemble for downscaled monthly climate normals over north america.* doi:

10.31223/X5CK6Z

Nakamura, H., & Wallace, J. M. (1990, May). Observed Changes in Baroclinic Wave Activity during the Life Cycles of Low-Frequency Circulation Anomalies. *Journal of the Atmospheric Sciences*, *47*(9), 1100–1116. Retrieved 2021-08-04, from https://journals.ametsoc.org/view/journals/atsc/47/9/1520-0469_1990_047_1100_ocibwa_2_0_co_2.xml doi: 10.1175/1520-0469(1990)047⟨1100:OCIBWA⟩2.0.CO;2

O'Gorman, P. A., & Schneider, T. (2009). The physical basis for increases in precipitation extremes in simulations of 21st-century climate change. *Proceedings of the National Academy of Sciences*, *106*(35), 14773-14777. Retrieved from https://www.pnas.org/doi/abs/10.1073/pnas.0907610106 doi: 10.1073/pnas.0907610106

Park, S., & Shin, J. (2019). *Snu sam0-unicon model output prepared for cmip6 cmip.* Earth System Grid Federation. Retrieved from https://doi.org/10.22033/ESGF/CMIP6.1489 doi: 10.22033/ESGF/CMIP6.1489

Reidmiller, D., Avery, C., Easterlng, D., Kunkel, K., Lewis, K., Maycock, T., & Stewart, B. (2018). *Impacts, risks, and adaptation in the united states: Fourth national climate assessment* (Vol. 2; Tech. Rep.). Washington, DC, USA: U.S. Global Change Research Program. doi: 10.7930/NCA4.2018.

Rupp, D. E., Abatzoglou, J. T., Hegewisch, K. C., & Mote, P. W. (2013). Evaluation of cmip5 20th century climate simulations for the pacific northwest usa. *Journal of Geophysical Research: Atmospheres*, *118*(19), 10,884-10,906. Retrieved from https://agupubs.onlinelibrary.wiley.com/doi/abs/10.1002/jgrd.50843 doi: https://doi.org/10.1002/jgrd.50843

Sillmann, J., Kharin, V. V., Zhang, X., Zwiers, F. W., & Bronaugh, D. (2013). Climate extremes indices in the cmip5 multimodel ensemble: Part 1. model evaluation in the present climate. *Journal of Geophysical Research: Atmospheres*, *118*(4), 1716-1733. Retrieved from https://agupubs.onlinelibrary.wiley.com/doi/abs/10.1002/jgrd.50203 doi: https://doi.org/10.1002/jgrd.50203

Swart, N. C., Cole, J. N., Kharin, V. V., Lazare, M., Scinocca, J. F., Gillett, N. P., ... Sigmond, M. (2019). *Cccma canesm5 model output prepared for cmip6 cmip.* Earth System Grid Federation. Retrieved from https://doi.org/10.22033/ESGF/CMIP6.1303 doi: 10.22033/ESGF/CMIP6.1303

Tarek, M., Brissette, F. P., & Arsenault, R. (2020). Evaluation of the era5 reanalysis as a potential reference dataset for hydrological modelling over north america. *Hydrology and Earth System Sciences*, *24*(5), 2527–2544. Retrieved from https://hess.copernicus.org/articles/24/2527/2020/ doi: 10.5194/hess-24-2527-2020

Tatebe, H., & Watanabe, M. (2018). *Miroc miroc6 model output prepared for cmip6 cmip.* Earth System Grid Federation. Retrieved from https://doi.org/10.22033/ESGF/CMIP6.881 doi: 10.22033/ESGF/CMIP6.881

Taylor, K. E., Stouffer, R. J., & Meehl, G. A. (2012). An overview of cmip5 and the experiment design. *Bulletin of the American Meteorological Society*, *93*(4), 485 - 498. Retrieved from https://journals.ametsoc.org/view/journals/bams/93/4/bams-d-11-00094.1.xml doi: 10.1175/BAMS-D-11-00094.1

Wehrli, K., Guillod, B. P., Hauser, M., Leclair, M., & Seneviratne, S. I. (2018). Assessing the dynamic versus thermodynamic origin of climate model biases. *Geophysical Research Letters*, *45*(16), 8471-8479. Retrieved from https://agupubs.onlinelibrary.wiley.com/doi/abs/10.1029/2018GL079220 doi: https://doi.org/10.1029/2018GL079220

Wieners, K.-H., Giorgetta, M., Jungclaus, J., Reick, C., Esch, M., Bittner, M., ... Roeckner, E. (2019). *Mpi-m mpiesm1.2-lr model output prepared for cmip6 cmip.* Earth System Grid Federation. Retrieved from https://doi.org/10.22033/ESGF/CMIP6.742 doi: 10.22033/ESGF/CMIP6.742

Wilcox, E. M., & Donner, L. J. (2007). The frequency of extreme rain events in satellite rain-rate estimates and an atmospheric general circulation model. *Journal of Climate*, *20*(1), 53 - 69. Retrieved from https://journals.ametsoc.org/view/journals/clim/20/1/jcli3987.1.xml doi: 10.1175/JCLI3987.1

Yukimoto, S., Koshiro, T., Kawai, H., Oshima, N., Yoshida, K., Urakawa, S., ... Adachi, Y. (2019). *Mri mri-esm2.0 model output prepared for cmip6 cmip.* Earth System Grid Federation. Retrieved from https://doi.org/10.22033/ESGF/CMIP6.621 doi: 10.22033/ESGF/CMIP6.621

Ziehn, T., Chamberlain, M., Lenton, A., Law, R., Bodman, R., Dix, M., ... Druken, K. (2019). *Csiro access-esm1.5 model output prepared for cmip6 cmip.* Earth System Grid Federation. Retrieved from https://doi.org/10.22033/ESGF/CMIP6.2288 doi: 10.22033/ESGF/CMIP6.2288

Acknowledgments

This work was supported by funding from the State of Washington. CMIP6 data was accessed using the Pangeo platform's data catalog (https://pangeo.io) Abernathey et al. (2017), which was supported by NSF Award 1740648. 152020Hersbach et al.Hersbach et al. () was downloaded from the Copernicus Climate Change Service (C3S) Climate Data Store.

CMIP6_bias.png.

(a)

(b)

−8 −6 −4 −2 0 2 4 6 8

Mean Bias (°C)

0 3 6 9 12 15 18 21

Model Count

Composite_SLP.png.

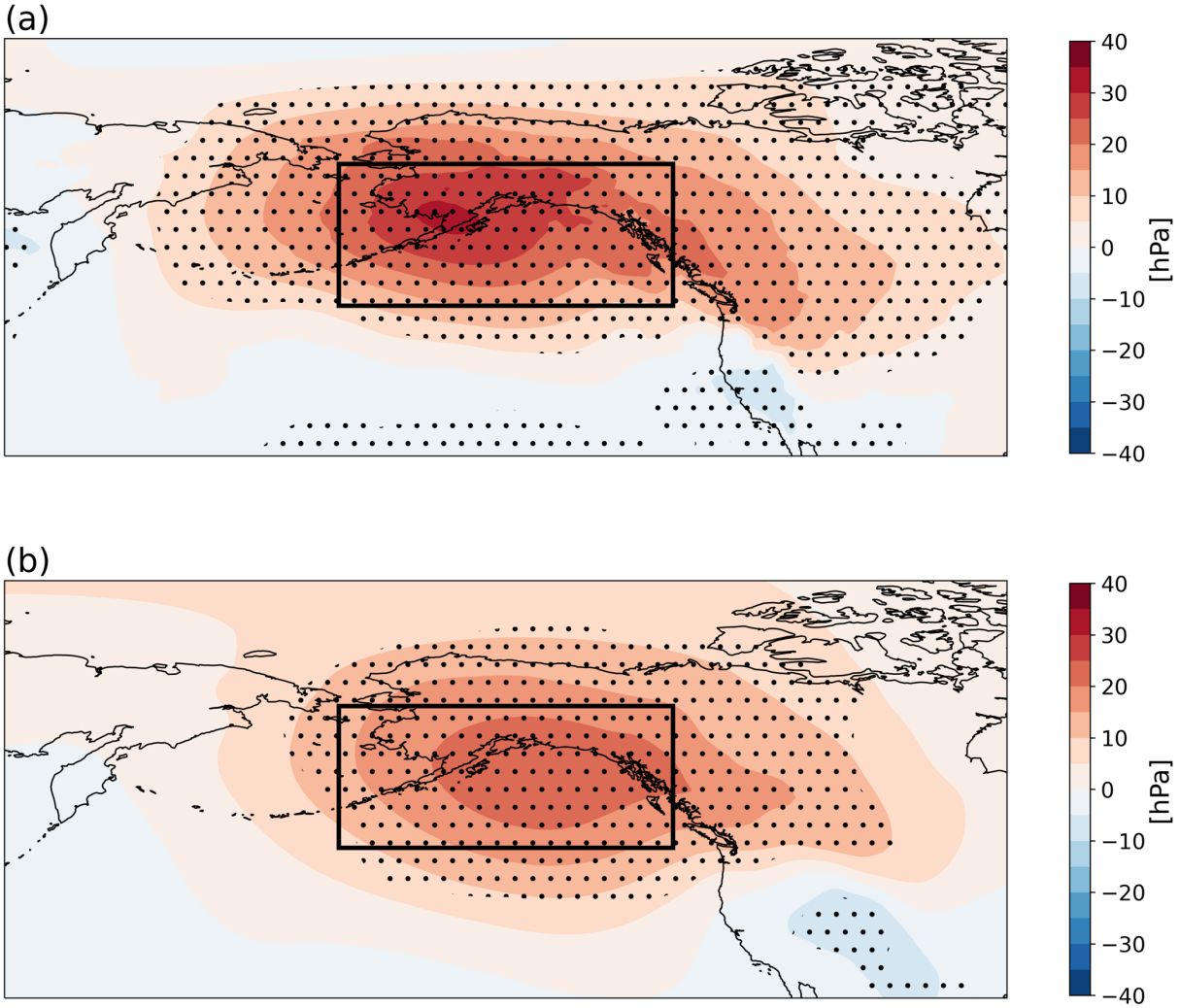
(a)
40
30
20
10
0
−10
−20
−30
−40
[hPa]
(b)
40
30
20
10
0
−10
−20
−30
−40
[hPa]

density.png.

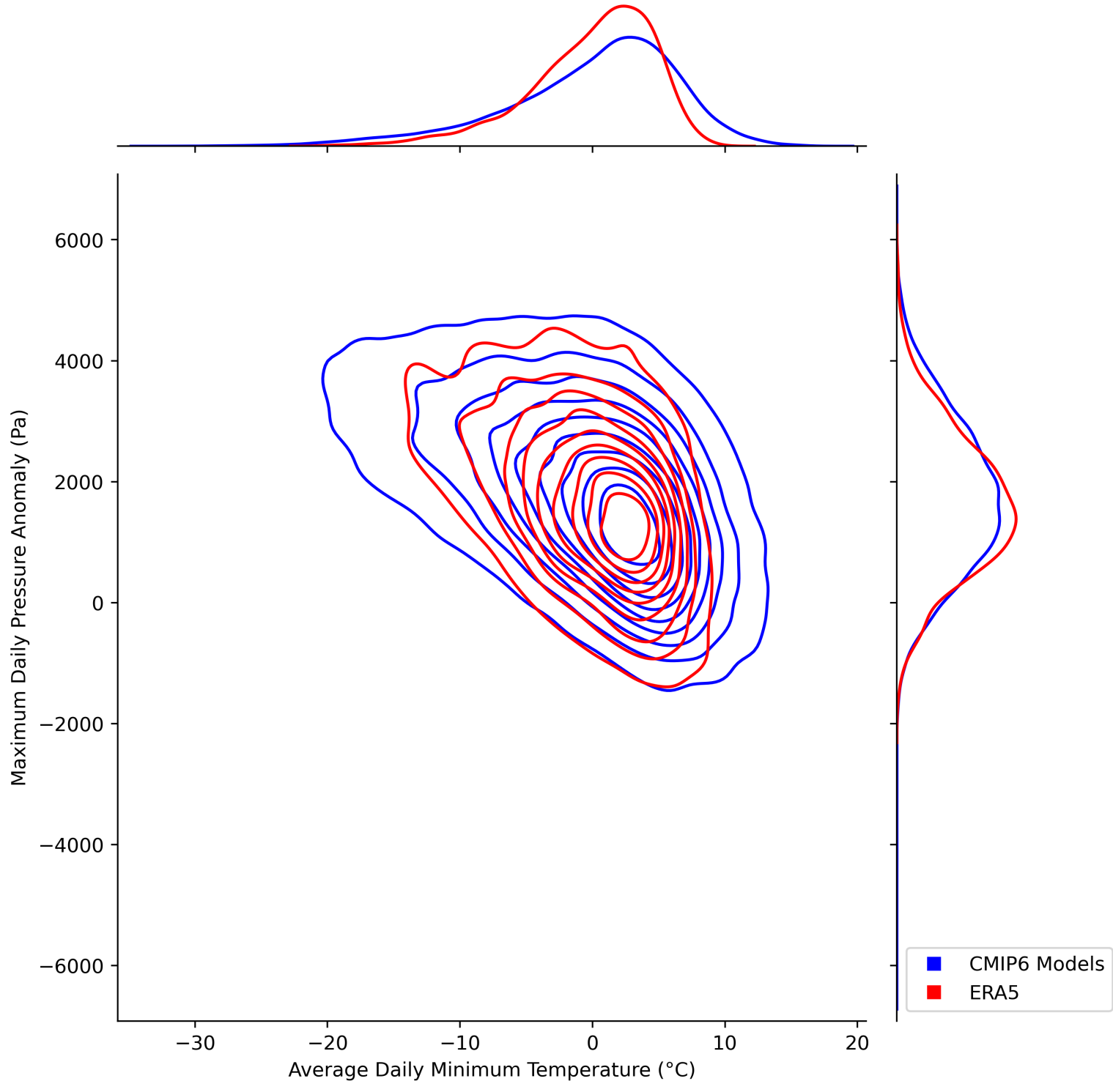
6000
4000
2000
0
−2000
−4000
−6000
Maximum Daily Pressure Anomaly (Pa)
−30
−20
−10
0
10
20
Average Daily Minimum Temperature (°C)
CMIP6 Models
ERA5

cross_section.png.

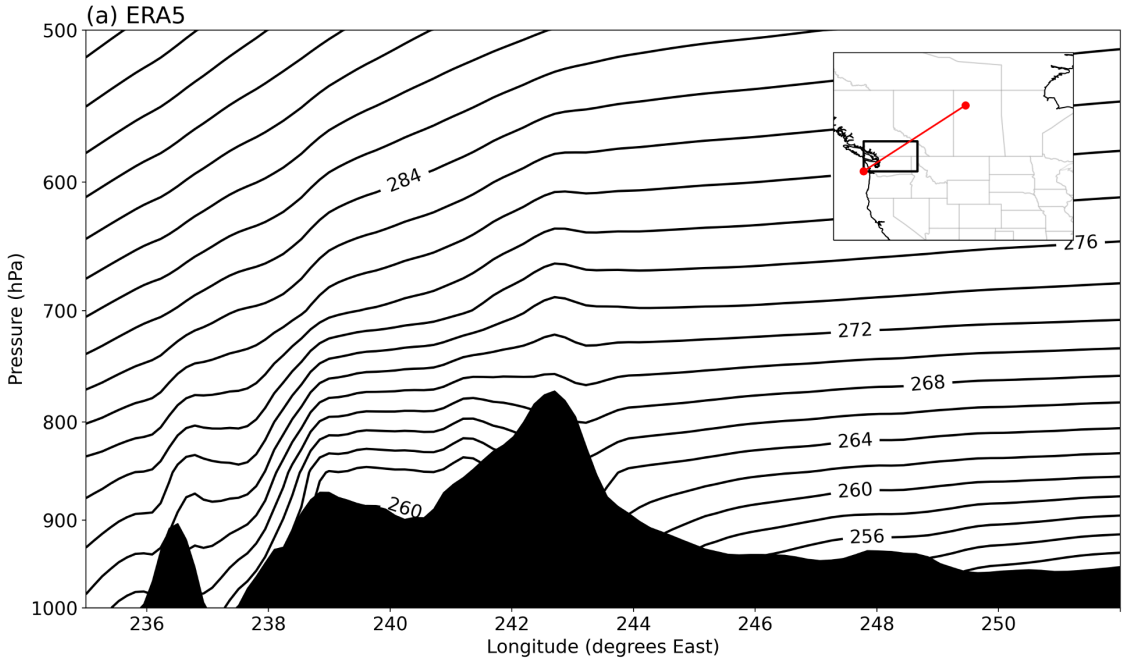
(a) ERA5
Pressure (hPa)
Longitude (degrees East)
500
600
700
800
900
1000
236
238
240
242
244
246
248
250
284
276
272
268
264
260
256

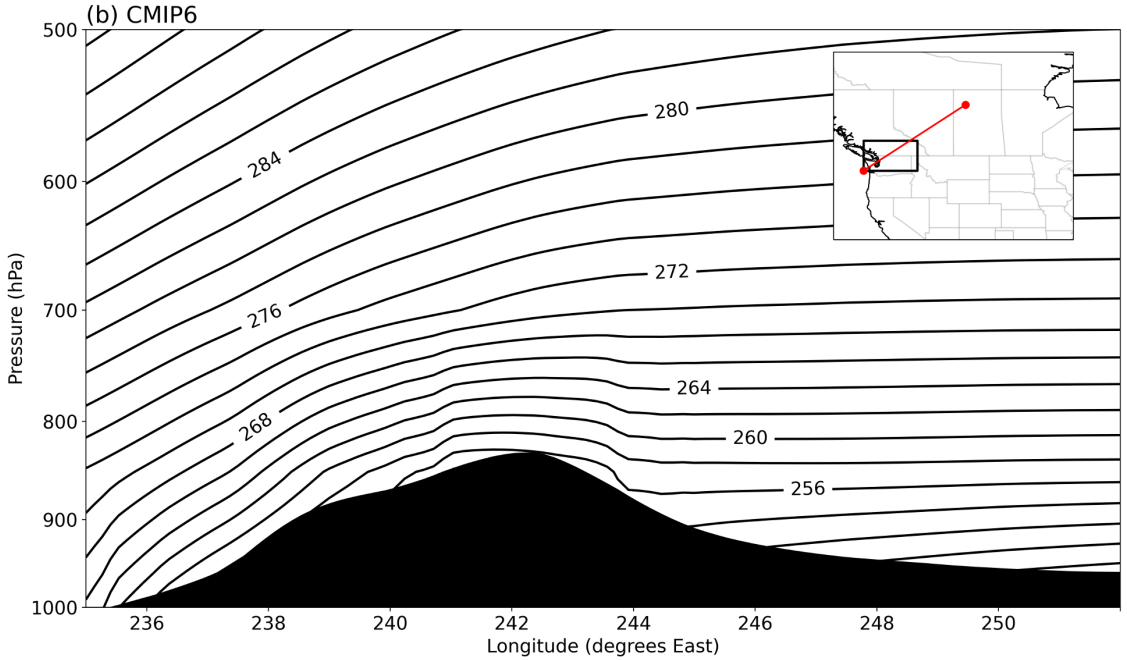
(b) CMIP6
Pressure (hPa)
Longitude (degrees East)
500
600
700
800
900
1000
236
238
240
242
244
246
248
250
280
284
276
272
268
264
260
256

orography.png.

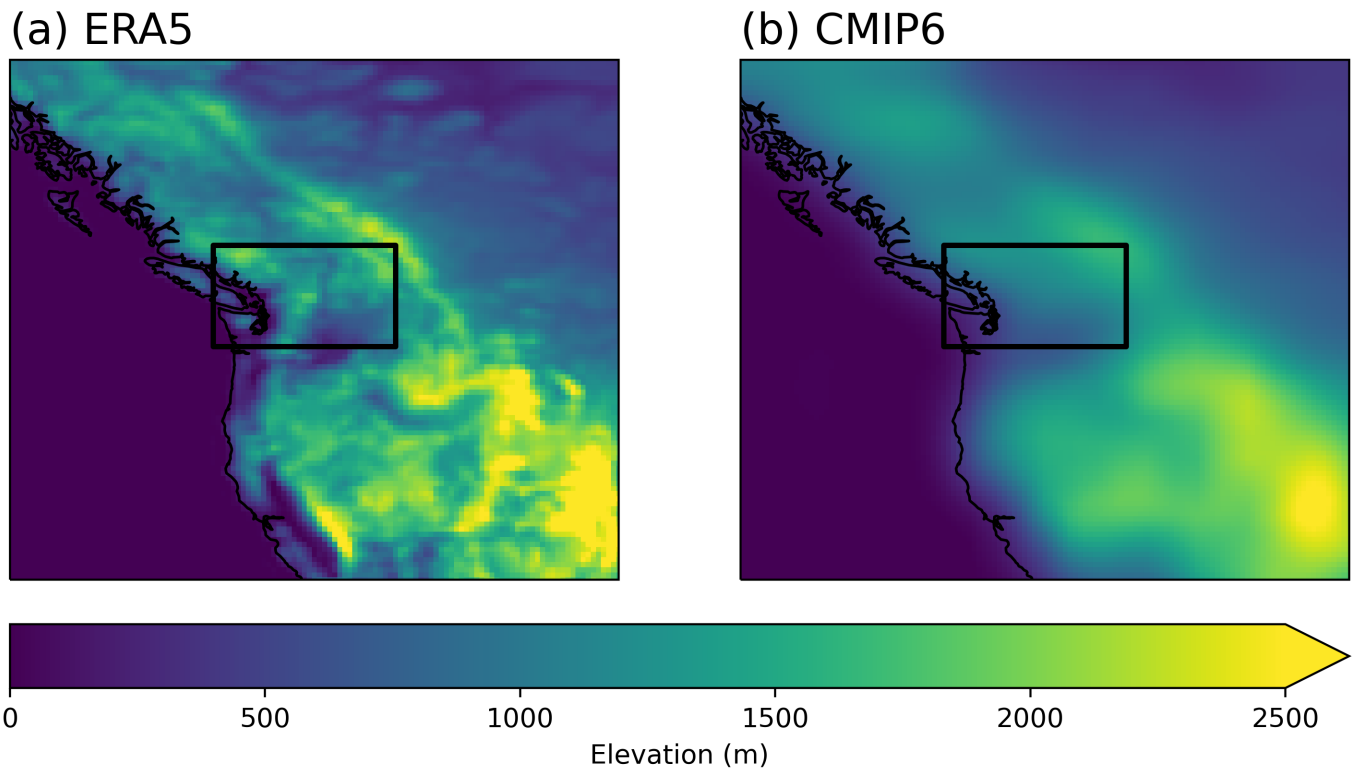
(a) ERA5
(b) CMIP6
0
500
1000
1500
2000
2500
Elevation (m)

tasmin_bias.png.

(a)

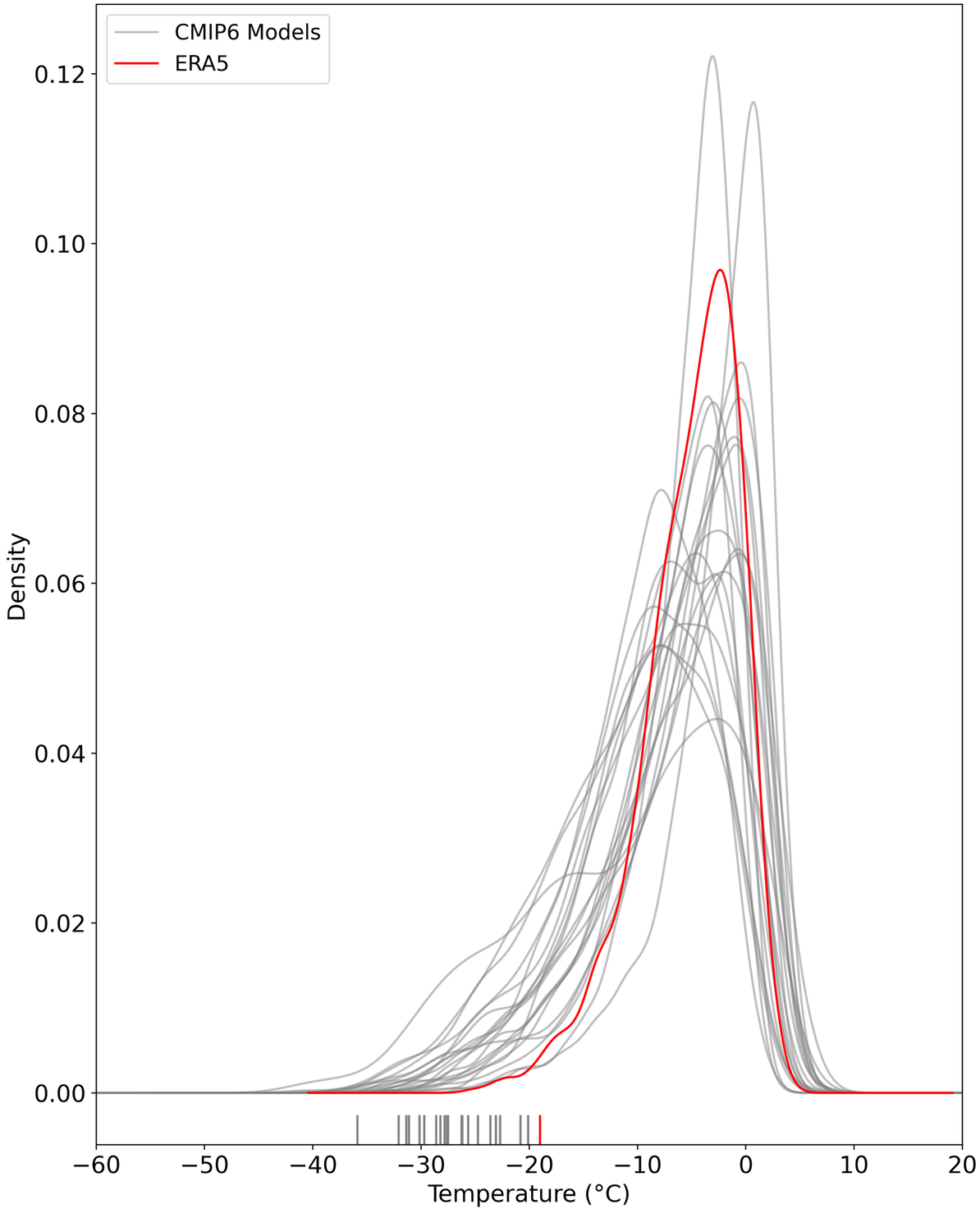
CMIP6 Models
ERA5
0.12
0.10
0.08
0.06
0.04
0.02
0.00
Density
−60
−50
−40
−30
−20
−10
0
10
20
Temperature (°C)

(b)

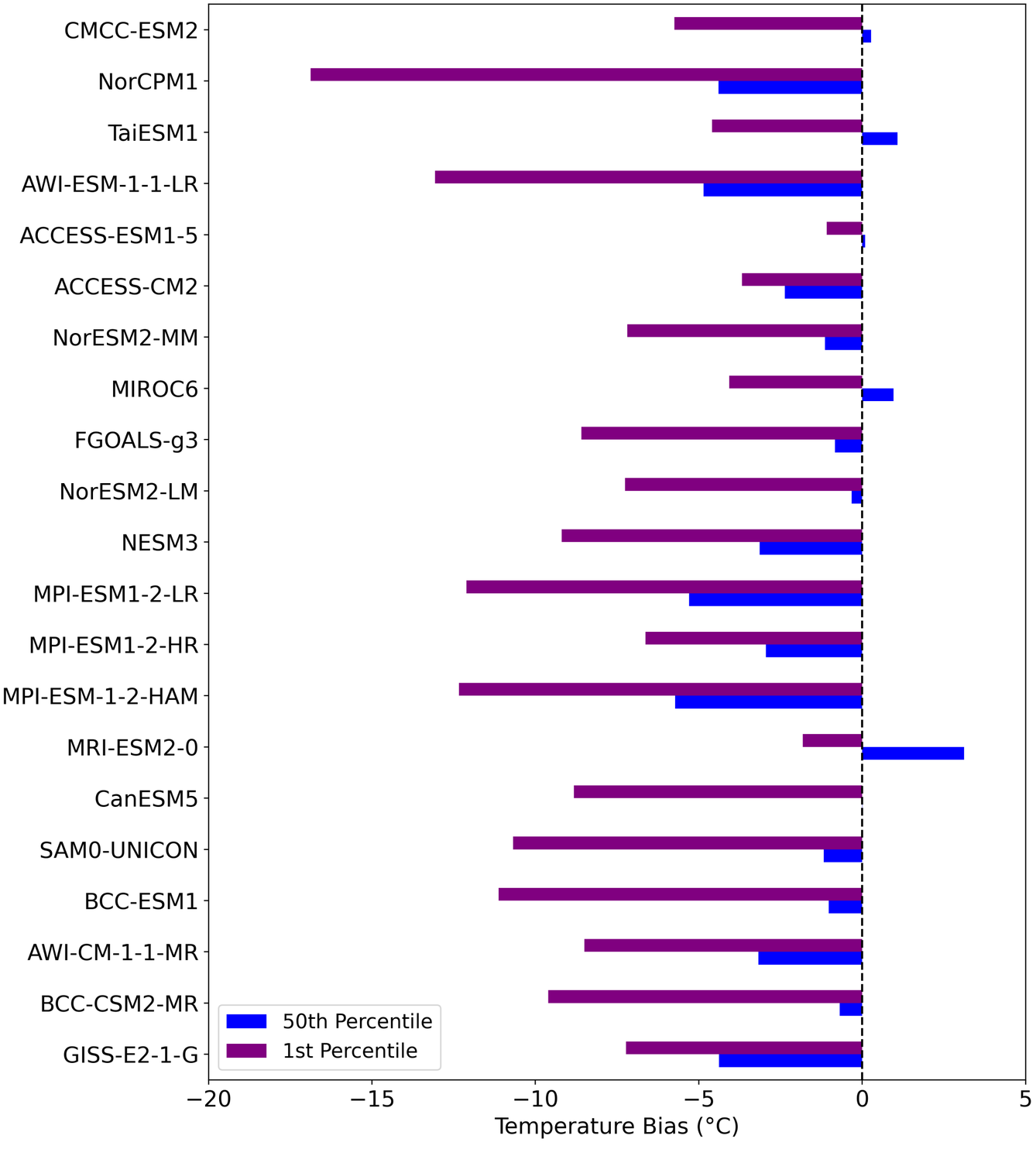
CMCC-ESM2
NorCPM1
TaiESM1
AWI-ESM-1-1-LR
ACCESS-ESM1-5
ACCESS-CM2
NorESM2-MM
MIROC6
FGOALS-g3
NorESM2-LM
NESM3
MPI-ESM1-2-LR
MPI-ESM1-2-HR
MPI-ESM-1-2-HAM
MRI-ESM2-0
CanESM5
SAM0-UNICON
BCC-ESM1
AWI-CM-1-1-MR
BCC-CSM2-MR
GISS-E2-1-G
50th Percentile
1st Percentile
−20
−15
−10
−5
0
5
Temperature Bias (°C)